Simple model of a planar undulating magnetic microswimmer

Emiliya Gutman and Yizhar Or*
Faculty of Mechanical Engineering, Technion - Israel Institute of Technology, Israel

One of the most efficient actuation methods of robotic microswimmers for biomedical applications is by applying time-varying external magnetic fields. In order to improve the design of the swimmer and optimize its performance, one needs to develop simple theoretical models that enable explicit analysis of the swimmer's dynamics. This paper studies the dynamics of a simple microswimmer model with two magnetized links connected by an elastic joint, which undergoes planar undulations induced by an oscillating magnetic field. The nonlinear dynamics of the microswimmer is formulated by assuming Stokes flow and using resistive force theory to calculate the viscous drag forces. Key effects that enable the swimmer to overcome the scallop theorem and generate net propulsion are identified, including violation of front-back symmetry. Assuming small oscillation amplitude, approximate solution is derived by using perturbation expansion, and leading-order expressions for the swimmer's displacement per cycle X and average speed V are obtained. Optimal actuation frequencies that maximize X or V are found for given swimmer's parameters. An ultimate optimal choice of swimmer's parameters and actuation frequency is found, for which the average swimming speed V attains a global maximum. Finally, the theoretical predictions of optimal performance values are validated by comparison to reported experimental results of magnetic microswimmers.

Recent technological progress in manufacturing of nano- and micro-systems has led to a growing interest in developing micron-scale robotic swimmers which are greatly inspired by locomotion capabilities of swimming microorganisms [1]. Such robots have a promising potential in biomedical applications, for performing tasks such as targeted drug delivery, intravenous tumor detection, and minimally invasive microsurgical operations [2]. One of the most efficient techniques for actuation of robotic microswimmers is by applying time-varying external magnetic fields [3]. The power density of magnetic actuation has been found suitable to micron-scale biomedical applications and simplifies the design of the swimmer, which does not have to carry energy resources and actuators. One of the pioneering prototypes of a magnetically-actuated microswimmer has been presented in 2005 by Dreyfus *et al* [4]. This microswimmer consists of a chain of spherical magnetic particles connected by flexible DNA links, and propulsion is generated by planar travelling-wave undulations of its body, which are induced by a planar oscillating magnetic field. Later on, other microswimmers have been designed, which are actuated by a rotating magnetic field that induces corkscrew-like propulsion [5, 6]. Some of these prototypes are made of rigid nano-helices [6, 7] some consist of particles connected by a flexible nanowire [5], and some even use an elastic filament made of real bacterial flagellum [8]. The dynamics of this type of microswimmers has recently been analyzed theoretically in [9–11]. While the aforementioned microswimmers maintain a constant rigid-body shape during their motion, the microswimmer of Dreyfus *et al* [4] employs a different mode of locomotion in which the swimmer's internal shape undergoes planar undulations. Such swimmers have been theoretically analyzed in [12–14], where the elastic body is modelled as a continuous deflecting beam. The resulting formulations are highly complicated and involve partial differential equations where most of the analysis is conducted for extreme cases, or by using numerical simulations. The goal of this work is to study a lumped-parameter simplified version of the microswimmer model in [4], which is amenable to explicit analysis that provides physical insights into the influence of governing physical parameters. Inspired by insights gained from Purcell's classical three-link swimmer [15–17] and later simplistic models such as [18–20], our model consists of only two rigid links connected by a passive elastic joint. This is perhaps the simplest possible model of a microswimmer which is capable of swimming by performing planar undulations induced by external magnetic actuation.

The microswimmer model is shown in Fig. 1(a). It consists of two elongated cylindrical links with equal lengths l and radii a. The links are connected by a flexible rotary joint with torsional spring constant k, so that the internal torque acting at the joint is given by $\tau = -k\phi$ where ϕ denotes the relative angle between the links. Only planar motion of the swimmer in x–y plane is considered, while all rotations are about the perpendicular direction $\hat{\mathbf{z}}$. The two links are magnetized such that the directions of their magnetization moments are aligned with the links' longitudinal axes, denoted by $\mathbf{t}_1$ and $\mathbf{t}_2$. The magnetization strengths of the two links are denoted by h_1 and h_2. A time-varying external magnetic field is applied, which is given by $\mathbf{B}(t)=b_x(1, \varepsilon \sin(\omega t))^T$. That is, $\mathbf{B}(t)$ has a constant component in x direction while its component in y direction is oscillating at a frequency ω. The external torque (moment) acting on the i^{th} link due to the magnetic field is given by $\mathbf{M}_i = h_i \mathbf{t}_i \times \mathbf{B}$, where magnetic dipole-dipole interaction between the two links is neglected for simplicity (it decays with the distance d as $1/d^3$). The swimmer is submerged in a Newtonian fluid with viscosity μ, and is assumed to be neutrally buoyant

*izi@tx.technion.ac.il

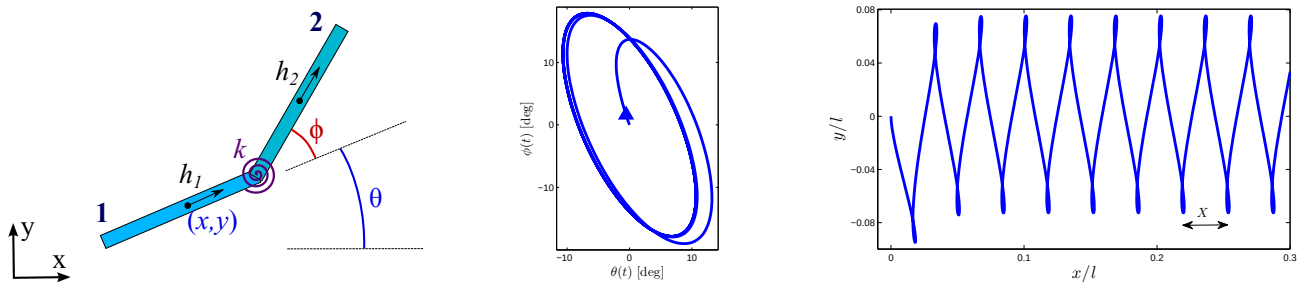

(a) (b) (c)

FIG. 1: (a) The two-link microswimmer model; Simulated trajectories: (b) in $\phi-\theta$ plane, and (c) in $x-y$ plane.

so that gravity has no effect on its motion. Due to its small scale, the swimmer is governed by low Reynolds number hydrodynamics where viscous forces dominate while inertial effects are negligible. The net forces and torques acting at the links' centers due to viscous drag are approximated by using resistive force theory for slender bodies [21, 22] as

$$\begin{aligned} \mathbf{f}_i &= -c_t l(\mathbf{u}_i \cdot \mathbf{t}_i)\mathbf{t}_i - c_n l(\mathbf{u}_i \cdot \mathbf{n}_i)\mathbf{n}_i \\ M_i &= -\frac{c_n l^3}{12}\omega_i \end{aligned} \tag{1}$$

for i=1, 2, where c_t=$\frac{2\pi\mu}{ln(l/a)}$ is the viscous resistance in the link's axial direction $\mathbf{t}_i$ and c_n=$2c_t$ is the viscous resistance in the normal direction $\mathbf{n}_i$, $\mathbf{u}_i$ is the linear velocity of the i-th link's center, and ω_i is its angular velocity.

Using terminology of robotic locomotion theory [23, 24], the robot's coordinates $\mathbf{q}$=$(\mathbf{q}_b, \phi)$ can be divided into body position variables $\mathbf{q}_b$ and shape variables, which in our model consist only of the joint angle ϕ. The body position is given by $\mathbf{q}_b$=(x, y, θ) where x, y are chosen as the position of link 1's center while θ denotes its orientation angle. Expressing the hydrodynamic forces/torques in (1) as a function of the coordinates $\mathbf{q}$ and velocities $\dot{\mathbf{q}}$, the conditions of zero net force and torque on each link then give rise to the nonlinear equations of motion of the swimmer, which have the general form:

$$\begin{aligned} \dot{\mathbf{q}}_b &= \mathbf{A}(\mathbf{q})\dot{\phi} + \mathbf{B}(\mathbf{q})\mathbf{F}_{ext} \\ \dot{\phi} &= \mathbf{C}(\mathbf{q})\mathbf{F}_{in} + \mathbf{D}(\mathbf{q})\mathbf{F}_{ext}\ , \end{aligned} \tag{2}$$

where $\mathbf{F}_{in}$ are internal actuation forces/torques at the joints (exerted by motors or springs), and $\mathbf{F}_{ext}$ denote external forcing terms (e.g. due to magnetic actuation or gravity). Combining the two equations in (2) and using the expressions for the magnetic torques and the torsion spring, the equation of motion can be rewritten in a more explicit structure that emphasizes the contribution of each effect as:

$$\dot{\mathbf{q}} = \mathbf{w}_0(\mathbf{q})k\phi + \mathbf{w}_1(\mathbf{q})\tau_1(\mathbf{q}, t) + \mathbf{w}_2(\mathbf{q})\tau_2(\mathbf{q}, t)\ , \tag{3}$$

where $\tau_i(\mathbf{q}, t) = h_i\hat{\mathbf{z}}\cdot(\mathbf{t}_i(\mathbf{q})\times\mathbf{B}(t))$ is the magnetic torque acting on the i^{th} link for $i = 1, 2$.

The structure of the equations of motion in (2) and (3) gives some insights about the swimming capabilities of this model, as follows. First, (2) indicates that in the absence of external forcing $\mathbf{F}_{ext}$=0, the swimmer can only perform reciprocal motion under bounded motion of the single shape variable $\phi(t)$. This is precisely the famous *scallop theorem* coined by Purcell [15]. An exception of this rule occurs when the angle ϕ is allowed to grow unbounded, and this is precisely the effect which is harnessed for generating forward motion of corkscrew-like swimmers such as *E. Coli* bacteria [15, 25] by constantly rotating a single actuated joint. The addition of external actuation $\mathbf{F}_{ext}$ enables the swimmer to overcome the scallop theorem and generate net motion even when the joint angle ϕ undergoes periodic oscillations, similar to the gravity-induced motion of the two-link swimmer model in [18]. Nevertheless, the structure of equation (3) indicates that adding external actuation is not always sufficient for swimming, since at least two of the three vector fields $\{\mathbf{w}_0(\mathbf{q}), \mathbf{w}_1(\mathbf{q}), \mathbf{w}_2(\mathbf{q})\}$ are required to have nonzero contribution in order to generate non-reciprocal motion. That is, the swimmer should at least have either an elastic joint and a single magnetized link, e.g. $k, h_1 \neq 0$ and h_2=0, or two magnetized link and a free joint, e.g. k=0 and $h_1, h_2 \neq 0$. Another special case, which cannot be directly seen from (3), occurs when the two links have equal magnetization strengths h_1=h_2 while $k > 0$. In this degenerate case where the swimmer possesses complete front-back symmetry, all solution trajectories of (3) converge asymptotically to the attractive invariant subspace ϕ=0, at which reciprocal motion is obtained with zero net motion. Physically, this motion corresponds to pure rotation of the swimmer about the hinge while the straightened configuration ϕ=0 is rigidly maintained but the joint exerts zero torque. This observation is closely related to the findings in [12, 13] which state that the front-back symmetry of the magnetic swimming filament must be somehow violated in order to generate net motion, either by local changes in elasticity or by attaching the large cargo (red blood cell) to the filament's end.

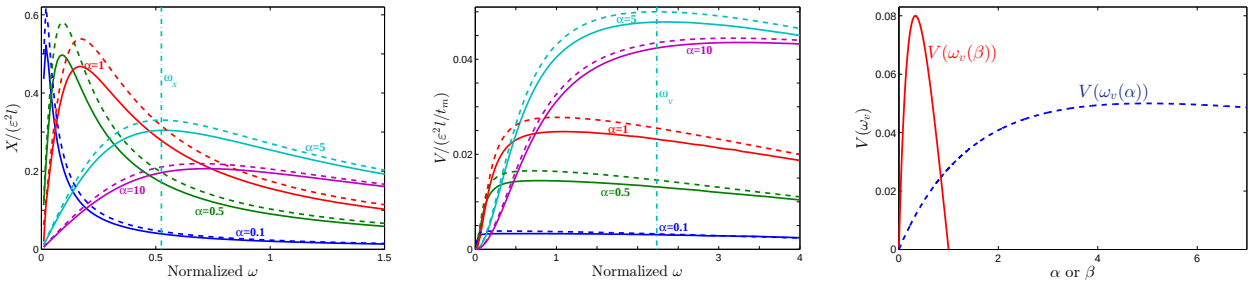

FIG. 2: Normalized (a) displacement $\frac{X}{\varepsilon^2 l}$ and (b) speed $\frac{V}{\varepsilon^2 l/t_m}$ vs ω for ε=0.4. Dashed curves are the leading-order expressions. Dash-dotted vertical lines are optimal frequencies ω_x and ω_v for α=5. (c) Maximal speed $V(\omega_v)$ normalized by $\varepsilon^2 l/t_m$, in case **I**– as a function of α (dashed), in case **II**– as a function of β (solid).

As a simulation example, numerical integration of (3) under initial conditions $\mathbf{q}(0)$=0 and parameter values of l=1, k=0.3, h_1=0, h_2=1, b_x=1, ε=0.4 and ω=1 produces the solution trajectories of $\mathbf{q}(t)$ in $\theta-\phi$ and $x-y$ planes as shown in Fig. 1(b) and 1(c), respectively. It can be seen that the solution of θ and ϕ rapidly converges to a periodic trajectory of cyclic undulation whereas the swimmer's linear motion consists of oscillations in y direction combined with net forward progress in x direction, which is aligned with the constant magnetic field b_x. Animation of this swimming motion is shown in the supplementary movie file [27]. The results demonstrate how external actuation combined with joint's elasticity enable this two-link microswimmer to overcome the scallop theorem and generate net forward displacement, as explained above.

In order to analyze the microswimmer's dynamics, we first identify characteristic time scales and use them to non-dimensionalize the equations of motion. The first time scale is associated with the response of a rigid straight swimmer with ϕ=0 and a single magnetized link, i.e. h_1=0, under a constant magnetic field, i.e. $\mathbf{B}=(b_x,0)^T$. In this case, the dynamics of the orientation angle $\theta(t)$ is obtained as $\dot{\theta}=-\frac{1}{t_m}\sin\theta$, where $t_m=\frac{4c_t l^3}{3b_x h_2}$ is the visco-magnetic characteristic time. For small initial orientations $\theta_0 \ll 1$, the angle decays to zero as $\theta(t)=\theta_0 e^{-t/t_m}$ so that the swimmer aligns with the direction of the constant magnetic field. Next, we consider the response of the swimmer's internal joint angle ϕ under zero magnetic field $\mathbf{B}$=0 and elastic spring $k>0$. In this case, the dynamics of the joint angle $\phi(t)$ is governed by the equation $\dot{\phi}=-\frac{6k(3+\cos\phi)}{c_t l^3(3-\cos\phi)}\phi$. Under small deviations from the equilibrium state ϕ=0, the solution decays as $\phi(t)=\phi_0 e^{-t/t_k}$ where $t_k=\frac{c_t l^3}{12k}$ is the visco-elastic characteristic time. In what follows, the time t is normalized by the characteristic time t_m, and the two nondimensional parameters $\alpha=t_m/t_k$ and $\beta=h_1/h_2$ are introduced. Without loss of generality, it is assumed that $|h_1|\le|h_2|$, which implies that $|\beta|\le 1$. We focus on three different cases: in case **I**, only one link of the swimmer is magnetized, β=0. In case **II**, both links are magnetized but there is no torsion spring at the joint, α=0. Finally, in case **III** there are two magnetized links and a torsion spring, i.e. $\alpha,\beta\neq 0$.

An important observation which has already been made in [4, 13] is that the swimmer's motion is significantly affected by the actuation frequency ω. As a numerical example, Figs. 2(a) and 2(b) plot the swimmer's net x-displacement per cycle X and the average speed $V=\frac{\omega}{2\pi}X$, respectively, as a function of ω for case **I** (β=0) and b_x=1, ε=0.4, under several values of α. Interestingly, it can be seen that for each value of α there exists an optimal frequency that maximizes X and a different optimal frequency that maximizes V. Moreover, a closer look into Fig. 2(b) indicates that there exists a unique combination of stiffness α and frequency ω for which the average speed V attains a global maximum.

In order to analytically study the influence of frequency and of the microswimmer's parameters on its performance, approximate expressions for the dynamics and its solution are obtained analytically under small oscillations of the external magnetic field, by using perturbation expansion [26]. Thus, it is assumed that $\varepsilon\ll 1$ and the solution $\mathbf{q}(t)$ of (2) is expanded into a power series in ε as $\mathbf{q}(t)=\varepsilon\mathbf{q}_{(1)}(t)+\varepsilon^2\mathbf{q}_{(2)}(t)+\varepsilon^3\mathbf{q}_{(3)}(t)+\ldots$. Since the dynamics of θ,ϕ in (3) is independent of the other components x,y, its first-order expansion in normalized time is obtained as the 2×2 linear system:

$$\begin{bmatrix}\dot{\theta}_{(1)}\\ \dot{\phi}_{(1)}\end{bmatrix}=\begin{bmatrix}-5\beta+3 & 0.5\alpha+3\\ 8\beta-8 & -\alpha-8\end{bmatrix}\begin{bmatrix}\theta_{(1)}\\ \phi_{(1)}\end{bmatrix}+\begin{bmatrix}5\beta-3\\ -8\beta+8\end{bmatrix}\sin(\omega t). \tag{4}$$

The solution of (4) consists of harmonic terms in ωt and transient terms of the form $c_i e^{\lambda_i t}$ where $\lambda_{1,2}$ are the eignevalues of the 2×2 matrix in (4). In order for the latter terms to decay to zero, the linear system in (4) is required to be asymptotically stable, i.e. $\mathrm{Re}(\lambda_{1,2})<0$. This implies two inequalities on the parameters α,β as

$$\alpha+5\beta+5>0 \quad\text{and}\quad \alpha+16\beta+\alpha\beta>0. \tag{5}$$

For cases **I** or **II**, the system is stable iff $\alpha>0$ or $\beta>0$,

respectively. This is because alignment of a magnetized link with the external field is equivalent to a stabilizing spring, hence the two angles θ, ϕ can be stabilized either by one torsion spring and one "magnetization spring" (case **I**), or by two "magnetization springs" (case **II**). Nevertheless, for case **III** where $\alpha, \beta \neq 0$, the stability conditions (5) are also met for some values where either $\alpha < 0$ or $\beta < 0$. The physical meaning of $\alpha < 0$ is that the torsional spring is *destabilizing*, i.e. $k < 0$, while $\beta < 0$ means that links' magnetization moments are in opposite directions.

Next, the leading-order solution for the swimmer's forward motion $x(t)$ is computed [28]. Using perturbation expansion of (2), it can be shown that the first-order solution for $x(t)$ vanishes since $\dot{x}_{(1)} = 0$, while its second-order dynamics is given by:

$$\dot{x}_{(2)} = \frac{l}{2}\left[-(\beta+1)\theta_{(1)}^2 - (\tfrac{1}{4}\alpha+3)\phi_{(1)}^2 + (\beta-4)\theta_{(1)}\phi_{(1)} + ((\beta+1)\theta_{(1)} + (-\beta+3)\phi_{(1)})\sin(\omega t)\right]. \tag{6}$$

Substituting the first-order solution of (4) into (6) and integrating in time, one obtains the solution for $x_{(2)}(t)$. Ignoring the transient terms that decay as $e^{\lambda_i t}$, the steady-state solution has the form:

$$x_{(2)}(t) = A(\omega,\alpha,\beta)\sin(2\omega t + \varphi(\omega,\alpha,\beta)) + \tilde{V}(\omega,\alpha,\beta)t. \tag{7}$$

That is, the leading-order expression for forward progress $x(t)$ consists of periodic terms in double frequency 2ω and a linear term which is precisely the swimmer's forward motion with average speed of $\varepsilon^2\tilde{V}$. It can also be shown that the third order dynamics of $x(t)$ vanishes due to symmetry considerations, i.e. $\dot{x}_{(3)}=0$. The explicit leading-order expressions for the average speed V and the net displacement per cycle $X=\frac{2\pi}{\omega}V$ are given by

$$\begin{aligned} X &= \varepsilon^2 l \frac{2\pi\omega(1-\beta)(\alpha+16\beta+\alpha\beta))}{\Psi(\omega,\alpha,\beta)} + O(\varepsilon^4) \\ V &= \varepsilon^2 \frac{l}{t_m}\frac{\omega^2(1-\beta)(\alpha+16\beta+\alpha\beta))}{\Psi(\omega,\alpha,\beta)} + O(\varepsilon^4) \end{aligned} \tag{8}$$

where

$$\Psi(\omega,\alpha,\beta) = \omega^4 + (\alpha^2+8\alpha\beta+8\alpha+25\beta^2+18\beta+25)\omega^2 + \alpha^2\beta^2 + 2\alpha^2\beta + \alpha^2 + 32\alpha\beta^2 + 32\alpha\beta + 256\beta^2.$$

These leading-order approximations of X and V as a function of ω are plotted as dashed curves in Figs. 2(a) and 2(b), respectively, for case **I** (β=0) with ε=0.4, under several values of α. Comparing to the values appearing in solid curves which were obtained from numerical integration, it is seen that the leading-order expressions are very good approximations that slightly over-estimate the exact values of X and V. When ε is further decreased, the discrepancy between the exact and approximate solutions is vanishing. The expressions in (8) also confirm the previous observation that the net forward motion vanishes in the cases where β=1, or α=β=0. Thus, at least one of two effects is necessary for swimming: either joint elasticity (case **I**) or two nonzero (yet unequal) links' magnetization strengths (case **II**).

Next, optimal actuation frequencies are derived. Using simple calculus for maximizing the expressions in (8), two different optimal actuation frequencies ω_x and ω_v (normalized by $1/t_m$) are found, for which X and V, respectively, are maximized. The optimal frequencies depend on the swimmer's parameters α and β as follows. Frequency ω_x is obtained as the positive real solution of the bi-quadratic equation

$$\begin{aligned} &3\omega_x^4 + (\alpha^2+8\alpha\beta+8\alpha+25\beta^2+18\beta+25)\omega_x^2 \\ &-\alpha^2\beta^2 - 2\alpha^2\beta - \alpha^2 - 32\alpha\beta^2 - 32\alpha\beta - 256\beta^2 = 0. \end{aligned} \tag{9}$$

Frequency ω_v is given by

$$\omega_v = \sqrt{\alpha + 16\beta + \alpha\beta}. \tag{10}$$

As an example, the values of ω_x=0.523 and ω_v=$\sqrt{5}$ in case **I** (β=0) for α=5 are plotted as the dash-dotted vertical lines in Figs. 2(a) and 2(b), respectively. One can see that X and V indeed attain maximal values at ω_x and ω_v.

Finally, we study optimization of the swimmer with respect to the parameters α and β. From Fig. 2(a), it can be seen that for case **I** (β=0), the maximal displacement $X(\omega_x)$ increases upon decreasing α, where an upper bound of $X(\omega_x) \approx 0.63 l\varepsilon^2$ is obtained for $\alpha \to 0$. Nevertheless, the optimal frequency from (9) is vanishing $\omega_x \to 0$ in a non-differentiable way at α=0, which implies infinitely long period times. Thus, the limiting case of α=0 is not only mathematically ill-defined, but also physically meaningless. Similar observation holds for $X(\omega_x)$ in cases **II** and **III**. On the other hand, the maximal speeds $V(\omega_v)$ as a function of α in case **I** and of β in case **II** are plotted in Fig. 2(c). It is clearly seen that there exist finite optimal choices of the parameters α or β for which $V(\omega_v)$ attains a global maximum. Moreover, the plot also indicates that in terms of larger speed V, case **II** is better than case **I**. As for the combined case **III** in which $\alpha, \beta \neq 0$, a contour plot of $V(\omega_v)$ in $\alpha-\beta$ plane is shown in Fig. 3. Again, it is seen that there exists a unique optimal choice of α and β which maximizes $V(\omega_v)$. The shaded region in the plot is the parameters region for which the straight solution of ϕ=θ=0 is unstable according to the inequalities in (5), indicating that the optimal point lies within the stable region. The optimal parameter values can also be found explicitly by simply applying multivariate calculus to the expression for V in (8), as follows. For case **I** where β=0, the optimal values are α=5 and ω_v=$\sqrt{5}$, and the resulting maximal speed is V=$0.05\varepsilon^2 l/t_m$. For case **II** where α=0, the optimal values are $\beta = \frac{1}{3}$ and $\omega_v = \frac{4}{\sqrt{3}}$, and the resulting maximal speed is $V = 0.08\varepsilon^2\frac{l}{t_m}$. Thus, using a swimmer with a free joint and optimal magnetization difference of 3:1 between the links gives an increase of 60% in the swimming speed compared to case **I** of a single

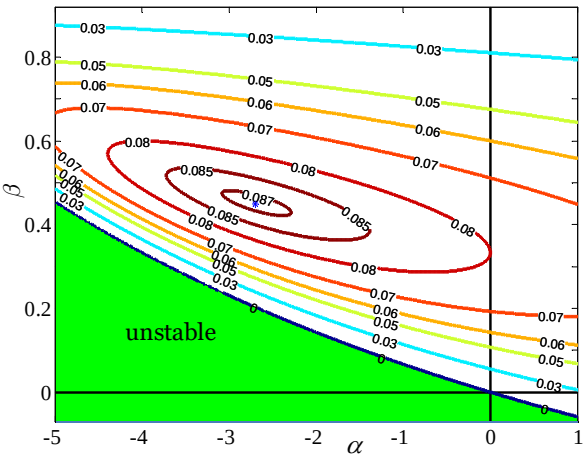

FIG. 3: Contour plot of the normalized swimming speed $\frac{V(\omega_v)}{\varepsilon^2 l/t_m}$ in $\alpha-\beta$ plane for case **III**.

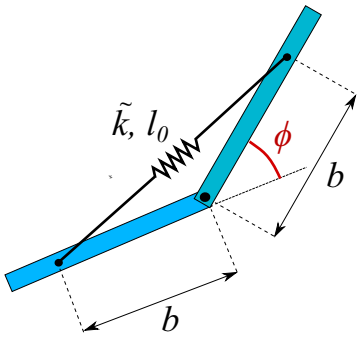

FIG. 4: A mechanical implementation of an effectively destabilizing torsion spring.

magnetized link and a torsion spring. That is, considering the isolated contribution of each of the two effects of elasticity α (case **I**) and magnetization of two links β (case **II**), the latter effect is much more significant. Finally, for case **III** where $\alpha, \beta \neq 0$, the optimal values are $\alpha \approx -2.7$, $\beta \approx 0.45$, $\omega_v \approx 1.82$, and the resulting maximal speed is $V \approx 0.0873\varepsilon^2 l/t_m$. Importantly, in this case the torsion spring is *destabilizing* ($\alpha < 0$), but the overall stability conditions (5) are still satisfied. That is, the fastest swimmer design consists of two unequally magnetized links and a destabilizing torsion spring. An example of implementing an effectively destabilizing torsion spring by using a pre-loaded linear spring is given below. While the design of such a mechanical arrangement in practice might be quite challenging, it results in a significant (9%) increase in swimming speed compared to case **II**.

We mow briefly discuss a possible mechanical implementation of an effectively destabilizing torsion spring, as shown in the two-link swimmer model in Fig. 4. The rotary joint is passive (torque-free), and a linear spring with stiffness constant $\tilde{k}$ and free length l_0 is connected to the two links at distances b from the joint. It is assumed that the plane of the linear spring is in offset from the links and the joint so that no interference occurs at $\phi = 0$. The elastic potential energy of the spring is given by $U(\phi)=\frac{1}{2}\tilde{k}(b\sqrt{2+2\cos\phi} - l_0)^2$. The torque exerted by the linear spring about the joint is $\tau(\phi)=-\frac{dU}{d\phi}$, and its Taylor expansion about $\phi=0$ is given by $\tau(\phi)=-\frac{1}{2}\tilde{k}b(l_0-2b)\phi+O(\phi^3)$. Thus, to leading order, the linear spring is equivalent to a torsion spring $\tau=-k\phi$ with effective first-order stiffness of $k=\frac{1}{2}\tilde{k}b(l_0-2b)$. One can see that if $l_0>2b$, i.e. the spring is under compression at $\phi=0$, then $k>0$ and the straightened configuration is stable. On the other hand, if $l_0<2b$, i.e. the spring is under tension at $\phi=0$, then $k<0$ and the straightened configuration is unstable. Thus, stability or instability of the effective torsion spring at $\phi=0$ is can be determined by the choice of the spring's unstressed length l_0.

Finally, we compare the results of our theoretical model to reported experimental results of robotic microswimmers from the literature. Importantly, note that comparison can only be made with swimmers in which the forward speed is proportional to ε^2, where $\varepsilon=b_y/b_x$ is the ratio of constant to oscillating/rotating components of the magnetic field. Therefore, all microswimmers composed of a rigid helix such as [6, 7], for which motion can be generated even for $b_x=0$, are not comparable to our model. We thus consider only two experimental microswimmers: the planar chain of DNA-linked beads of Dreyfus *et al* [4, 13] and the flexible rotating nanowire of Pak *et al* [5]. Each of these microswimmers is actuated at a frequency $f=\omega/2\pi$ in Hz, which is the frequency of oscillations (Dreyfus) or rotation (Pak). The reported swimming speeds V are normalized by the total body length L and the frequency f. The resulting quantity V/Lf is precisely the net displacement per period X. Two optimal values were reported for each microswimmer – maximal normalized speed V/Lf which is equivalent to maximal displacement X^*, and maximal speed V^*. These two maximal values were attained at two different frequencies, f_x and f_v. This observation agrees with the theoretical prediction of our model, see Figs. 2(a)-(b). The reported maximal displacements X^* were compared to the results of our theoretical model for which $L=2l$, where X attains an upper bound of $X^*\approx 0.31\varepsilon^2 L$ at the non-physical limit of vanishing frequency $\omega_x \to 0$. The reported maximal speeds V^* were compared to the theoretical upper bound of $V^*/Lf_v \approx 0.15\varepsilon^2$, which was obtained in case **III** where $\alpha, \beta \neq 0$. Comparison of the results is summarized in Table I. One can see that the reported experimental values of maximal displacement and speed are below the optimal values according to our theoretical model, yet they are in the same order of magnitude. Nevertheless, we have found it difficult to draw concrete guidelines for practically improving the performance of the microswimmers prototypes by modification of their structure, elasticity, and/or actuation frequency. The main reason for this difficulty was our inability to obtain physical values of the visco-magnetic characteristic time t_m and visco-elastic time t_k for the microswimmers

Microswimmer	L (μm)	ε=b_y/b_x	$\frac{X^*}{\varepsilon^2 L}$	f_x (Hz)	$\frac{V^*}{\varepsilon^2 L f_v}$	f_v (Hz)
Dreyfus *et al* [4, 13]	24	10.3/8.9 =1.16	0.068	10	0.031	4
Pak *et al* [5]	5.8	10/9.5 =1.05	0.149	15	0.093	35
Our model	$2l$		0.31	$\omega_x \to 0$	0.15	$0.29/t_m$

TABLE I: Comparison of experimental magnetic microswimmers to our theoretical model. (For the microswimmer of Dreyfus *et al*, values of X^* and f_x are taken from [4] and from Table 1 in [5], while values of V^* and f_v are taken from [13].)

in [4, 5, 13], since it was impossible to extract data about the analogues of particles' magnetization h_i, lumped torsion stiffness k and resistive drag coefficient c_t. Thus, we could not match the reported optimal frequencies f_x and f_v in [4, 5, 13] to the theoretical values predicted by our model.

In summary, we have introduced the simplest possible model of a microswimmer which swims by performing planar undulations induced by external magnetic actuation. Using resistive force theory and perturbation expansion under small-amplitude oscillations, the nonlinear dynamics of the swimmer has been formulated, and dependence of the swimmer's performance on its physical parameters and actuation frequency has been explicitly analyzed. Optimal frequencies that maximize displacement per cycle X or average speed V for a given swimmer has been found, and optimal choices of swimmer's parameter that give fastest swimming were derived. It has been found that the effect of difference in links' magnetization on V is more significant than that of elasticity, and that the fastest swimmer consists of a combination of unequally magnetized links and a destabilizing torsion spring. Comparison of the theoretical predictions with reported experimental results of magnetically-actuated microswimmers suggests that their performance is suboptimal and improvements might be possible.

Many effects which are present in every realistic biomedical microswimmer have been neglected in our simplistic model, including hydrodynamic and magnetic interactions, dragging a large cargo, elasticity of a continuous filament, and non-Newtonian fluid rheology. While extensions that account for some of these features are currently under our investigation, conveying the results and insights learnt from simplistic mathematical models into efficient design, optimization and control of real microswimmers remains a challenging and important open problem in this research field.

[1] E. Lauga and T. R. Powers, Rep. Prog. Phys. **72**, 096601 (2009).
[2] B. J. Nelson, I. K. Kaliakatsos, and J. J. Abbott, Annual Review of Biomedical Engineering **12**, 55 (2010).
[3] K. E. Peyer, L. Zhang, and B. J. Nelson, Nanoscale **5**, 1259 (2013).
[4] R. Dreyfus, J. Baudry, M. L. Roper, M. Fermigier, H. A. Stone, and J. Bibette, Nature **437**, 862 (2005).
[5] O. S. Pak, W. Gao, J. Wang, and E. Lauga, Soft Matter **7**, 8169 (2011).
[6] A. Ghosh and P. Fischer, Nano Letters **9**, 2243 (2009).
[7] L. Zhang, J. A. Abbott, L. Dong, K. E. Peyer, B. E. Kratochvil, H. Zhang, C. Bergeles, and B. J. Nelson, Nano Letters **9**, 3663 (2009).
[8] U. K. Cheang, D. Roy, J. H. Lee, and M. J. Kim, Applied Physics Letters **97**, 213704 (2010).
[9] Y. Man and E. Lauga, Physics of Fluids **25**, 071904 (2013).
[10] K. I. Morozov and A. M. Leshansky, Nanoscale **6**, 1580 (2014).
[11] K. E. Peyer, L. Zhang, B. E. Kratochvil, and B. J. Nelson, in *Proc. IEEE Int. Conf. on Robotics and Automation* (2010), pp. 96–101.
[12] M. L. Roper, R. Dreyfus, J. Baudry, M. Fermigier, J. Bibette, and H. A. Stone, J. Fluid Mech. **554**, 167 (2006).
[13] M. Roper, R. Dreyfus, J. Baudry, M. Fermigier, J. Bibette, and H. Stone, Proc. Roy. Soc. A pp. 877–904 (2008).
[14] M. Belovs and A. Cēbers, Physical Review E **79**, 051503 (2009).
[15] E. M. Purcell, Am. J. Phys. **45**, 3 (1977).
[16] L. E. Becker, S. A. Koehler, and H. A. Stone, J. Fluid Mech. **490**, 15 (2003).
[17] J. E. Avron and O. Raz, New J. Phys. **10**, 063016 (2008).
[18] L. J. Burton, R. L. Hatton, H. Choset, and A. E. Hosoi, Physics of Fluids **22**, 091703 (2010).
[19] Y. Or, Phys Rev. Lett. **108**, 258101 (2012).
[20] E. Passov (Gutman) and Y. Or, European Physical Journal E **35**, 78 (2012).
[21] J. Gray and G. J. Hancock, J. Exp. Biol. **32**, 802 (1955).
[22] R. G. Cox, J. Fluid Mech. **44**, 791 (1970).
[23] S. D. Kelly and R. M. Murray, J. of Robotic Systems **12**, 417 (1995).
[24] J. Ostrowski and J. Burdick, International Journal of Robotics Research **17**, 683 (1998).
[25] H. C. Berg, *E. Coli in Motion* (Springer-Verlag, NY, 2004).
[26] A. H. Nayfeh, *Perturbation methods* (Willey-VCH, 2004).
[27] A movie file is submitted online.
[28] The solution for $y(t)$ is less interesting, and is omitted due to space constraints. It can be shown that net motion in y direction vanishes due to the swimmer's symmetry.